Separation and Purification Technology 330 (2024) 125246

Contents lists available at ScienceDirect

Separation and Purification Technology

journal homepage: www.elsevier.com/locate/seppur

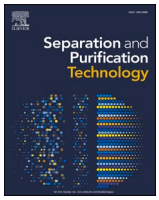

Environmentally safe ZVI/ZnS-based polymer composite for lindane degradation in water: Assessment of photocatalytic activity and eco-toxicity

Raffaella Rescigno [a], Olga Sacco [a,*], Stefania Pragliola [a], Luisa Albarano [b], Giovanni Libralato [b], Giusy Lofrano [c,*], Vincenzo Romano Spica [c], Olimpia Tammaro [d], Giorgia Montalbano [d], Serena Esposito [d], Vincenzo Vaiano [e], Vincenzo Venditto [a]

[a] Department of Chemistry and Biology "A. Zambelli", INSTM Research Unit, University of Salerno, via Giovanni Paolo II, 132, 84084 Fisciano (Salerno), Italy
[b] Department of Biology, University of Naples Federico II, Monte Sant'Angelo University Complex - Building 7, Via Vicinale Cupa Cintia 26, 80126 Naples, Italy
[c] Department of Movement, Human and Health Sciences, University of Rome Foro Italico, Piazza Lauro De Bosis, 15, 00135 Roma, Italy
[d] Department of Applied Science and Technology and INSTM Unit of Torino – Politecnico, Politecnico di Torino, Corso Duca degli Abruzzi 24, 10129, Torino, Italy
[e] Department of Industrial Engineering, INSTM Research Unit, University of Salerno, via Giovanni Paolo II, 132, 84084 Fisciano (Salerno), Italy

ARTICLE INFO

Editor: C. Han

Keywords:
ZVI/ZnS polymer composite
Polymeric aerogel
Lindane
Photocatalytic degradation
Toxic and genotoxic effects

ABSTRACT

Monolithic composite aerogel based on a photocatalytic system, constituted by Fe^0 (ZVI) coupled with ZnS (FZ), embedded into syndiotactic polystyrene (sPS) matrix was used, for the first time, in the lindane degradation under UV light. The content of FZ photocatalyst inside the monolithic composite aerogel (FZsPS) composite was 3 wt%. FESEM images of FZsPS indicate that the FZ photocatalyst is well dispersed in the polymer matrix. EDS analyses and temperature-programmed reduction (TPR-H_2) measurements revealed an interpenetrated structure of the ZVI and ZnS phases as well the presence of some iron in an oxidized form. Photocatalytic activity data showed that in presence FZsPS aerogel, the almost complete lindane degradation was achieved after only 30 min of UV irradiation time. FZsPS was also effective in the lindane mineralization since a TOC removal of about 94 % was detected after 180 min of treatment time. Remarkably, based on the toxicity evaluation on *Artemia franciscana*, while the bare FZ photocatalyst showed significant toxicity per se, no toxicity or genotoxicity was found in the water treated with the FZsPS composite system where FZ is immobilized into the sPS aerogel matrix. Therefore the proposed composite photocatalyst can be considered as a model for a strategy to eliminate the environmental impact of catalysts that would otherwise be harmful to water.

1. Introduction

Lindane is the common name of the γ-isomer of hexachlorocyclohexane (HCH), an organochlorine pesticide (OCP) widely used from 1950 s to 1980 s for both agricultural and non-agricultural purposes (USEPA, 2006 [1]). It has been used for example on fruits and vegetables, to control insects and pests, but also for seed and soil treatment, for the treatment of trees and wood, especially in coniferous forests and for the treatment against ectoparasites in both veterinary and human applications [2–4]. Its global production was around 600,000 tonnes during the period from 1950 s to 2000 s [5]. Italy was one of the top 10 countries with the highest usage of Europe [6].

The persistence of lindane in aquatic environments has been widely documented, as well as its toxicity to aquatic organisms [7]. The (L(E)C50) and chronic (NOEC) toxicity values are at the level of μg/L for several type of fishes and aquatic invertebrates. Several concerns have been reported regarding human health. AMAP reported an increase in HCH isomers in human tissues and breast milk [8]. It has been identified as a potential endocrine-disrupting chemical [9]. The United States Environmental Protection Agency (US EPA) and the World Health Organization (WHO) classify lindane as a potent carcinogen and teratogen agent [10,11]. The International Agency for Research on Cancer (IARC) has associated its exposure with one of the causes of non-Hodgkin's lymphoma (NHL) (IARC, 2016).

For these reasons, lindane was listed within the persistent organic pollutants by the 2009 Stockholm Convention [12]. As a result, its production and agricultural use were banned in more than 50 countries worldwide by 2010 [5], but pharmaceutical use is permitted as a second-line treatment for scabies and lice [13]. Therefore, HCH concentrations have been detected in water bodies all over the world (ranging from

* Corresponding authors.
E-mail addresses: osacco@unisa.it (O. Sacco), giusy.lofrano@uniroma4.it (G. Lofrano).

https://doi.org/10.1016/j.seppur.2023.125246
Received 3 August 2023; Received in revised form 15 September 2023; Accepted 28 September 2023
Available online 30 September 2023

0.087 to 5509 μg/L), as well as in drinking water, also due to its strong refractory degradation [14], becoming a concern of global relevance.

Traditional methods require long treatment times for lindane degradation because it is a hydrophobic organic molecule (logKow > 3.5) [15,16]. Thus, much effort is being made in developing more efficient and sustainable technologies to remove lindane from water.

Among several processes allowing the breaking of the C-Cl bond, technologies based on zero-valent iron (ZVI), which reacts with halogenated organic pollutants (RX) acting as a very powerful reducing agent [17], result as the most promising. In recent decades, the use zero-valent iron (ZVI) has been proposed for depolluting soils and aquifers because ZVI is highly reactive and inexpensive [18,19]. However, the halogenated organic pollutants degradation rates in presence of ZVI decrease over time [20] because Fe^0 is easily oxidized to Fe^{2+} [21] according to the following general reaction [21–24]:

$$Fe^0 + RX + H^+ = Fe^{2+} + RH + X^-$$

On the other hand, advanced oxidation processes (AOPs), such as heterogeneous photocatalysis, can degrade organic pollutants into harmless end products, including lindane [13,25–28], but the degradation performance is generally low when photocatalysis is used for the treatment of water polluted by chlorinated organic compounds (such as perchloroethylene and lindane) [26,29–33]. Indeed, in the case of lindane, it is reported that treatment times higher than 2 h are required for the almost complete pollutant degradation. Hence to improve the efficiency of photocatalytic processes for the degradation of halogenated organic pollutants, some authors have proposed to couple semiconductor photocatalysts, such as TiO_2, ZnO, g−C_3N_4 and g−C_3N_4/MoS_2, with ZVI to simultaneously exploit the photocatalytic degradation properties with the reductive action of ZVI [34–38]. In this perspective, Sacco et al. selected ZnS as a suitable semiconductor to be coupled with ZVI and demonstrated as it is possible to obtain a powder composite capable of degrading chlorobenzene more efficiently than ZnS and ZVI alone, evidencing that the simultaneous presence of UV light and ZnS avoid the ZVI oxidative corrosion phenomena, also preserving a high reactivity after several reuse cycles [39]. However, despite the interesting degradation performances reported by such photocatalytic composites, it must be considered that they have been used in slurry photoreactors in which the catalytic powders are dispersed within the aqueous medium. Therefore, the need for a post-treatment step for the separation of catalysts from the treated water remains the main constraint to the full-scale application of photocatalytic systems [40–43]. Moreover, the use of suspended particles for wastewater treatment implies their possible release into the environment, inducing a health risk due to the possible toxicity of these nanoparticles [44–49].

To overcome these drawbacks, the catalytic materials could be immobilized on the surface of suitable macroscopic supports [50,51] or dispersed within the porous structure of supports having a high affinity towards the target pollutant [52,53].

To date, among the different supports for photocatalysts (such as glass, ceramic or zeolites [54–56]) polymers are attracting more and more attention in the literature concerning heterogeneous photocatalysis [57–60].

Recent research papers reported that monolithic syndiotactic polystyrene (sPS) aerogels are promising supports for photocatalytic applications due to their good mechanical properties and the nanoporous crystalline phase which confers high surface areas and good sorption properties [59,61–66].

This research aimed at investigating for the first time the behavior of a composite aerogel (FZsPS) based on sPS and Fe^0/ZnS, in the photocatalytic degradation of lindane. The kinetic of degradation was fully characterized from a chemical and ecotoxicological viewpoint. In particular, embryo-larval and adult-related effects on *Artemia franciscana* were evaluated. Genotoxicity testing was also performed to determine potential hazards for direct or indirect DNA interaction.

It is worthwhile to note that to date no scientific paper reports toxicological results on the treated water coming from the photocatalytic degradation of lindane by using composite aerogels.

2. Materials and methods

2.1. Materials

Sodium borohydride ($NaBH_4$), zinc sulfide (ZnS) particles, iron (II) sulfate heptahydrate ($FeSO_4{\cdot}7H_2O$) and Lindane ($C_6H_6Cl_6$) were provided by Sigma–Aldrich. Syndiotactic polystyrene (sPS) used for the aerogels preparation was purchased from Idemitsu Kosan Co., Ltd. under the trademark XAREC© 90ZC.

2.2. Preparation of Fe^0 and Fe^0/ZnS photocatalyst

Fe^0/ZnS (FZ) photocatalyst in powder form were prepared following the procedure reported by Sacco et al. [39]. Specifically, 1 g of ZnS was added to 100 mL of distilled water where 4 g of $FeSO_4{\cdot}7H_2O$ was previously dissolved. The suspension was stirred for 10 min in the presence of an N_2 stream (flow rate: 30 NL/h) to remove dissolved oxygen. Subsequently, 1.4 g of reducing agent ($NaBH_4$) was added to the suspension, which was stirred in the presence of N_2 flow for 1 h, washed three times with ethanol and finally dried at room temperature overnight to obtain the FZ sample (Fe^0 content in the FZ photocatalyst was 45 wt% [39]).

Fe^0 particles were prepared following the same procedure but without adding ZnS in the aqueous solution.

FZ, ZnS and Fe^0 particles were deeply characterized in our previous work [39]. In detail, Wide-angle X-ray diffraction (WAXD) analysis of FZ evidenced diffraction patterns (at $2\theta = 28.6$, 33.2, 47.6 and 56.5°) due to ZnS [67,68]. Moreover, the characteristic peak of Fe^0, at about $2\theta = 45°$, was also detectable [39] with no signals related to iron oxides whose presence was instead shown by Raman spectra [39].

2.3. Preparation of FZsPS monolithic composite aerogel

The monolithic composite aerogel (FZsPS) was prepared according to the experimental procedure described by Sacco et al. [66]. Syndiotactic polystyrene (sPS) and the FZ photocatalyst with a weight ratio of 97/3 were dispersed in chloroform (chloroform/sPS weight ratio equal to 90/10) and inserted in a hermetically sealed test tube, which was then heated up to 100 °C. The formation of a gel was obtained after cooling the suspension from 100 °C to room temperature. The chloroform was extracted from the obtained gel through treatment with supercritical carbon dioxide (using an ISCO SFX 220 extractor) for 3 h at 40 °C and at a pressure of 20 MPa, obtaining the FZsPS monolithic composite aerogel in a cylindrical shape (diameter = 5.6 mm; height = 3 cm) (Figure S1 of Supplementary Material).

The content of FZ photocatalyt inside the FZsPS composite was 3 wt %.

Only for toxicity data analysis, monolithic composite aerogels containing Fe^0 and ZnS particles at 3 wt% (named Fe^0sPS and ZsPS, respectively) were also prepared with the same method used for the preparation of FZsPS.

2.4. Characterization techniques

Wide-angle X-ray diffraction (WAXD) patterns of the photocatalysts were obtained with a Brucker D8 Advance diffractometer, using a nickel filtered Cu-Kα radiation and Bragg–Brentano θ–θ geometry. The 2θ acquisition interval was 5–80°, with a step size of 0.0303° and a scanning acquisition time of 0.200 s/point.

To investigate the effect of iron on optical properties of ZnS powder, a Perkin Elmer Spectrofluorometer LS55 was used to collect the photoluminescence spectra with an excitation wavelength λex = 285 nm and slits 10 nm, recorded in the λ range of 300–550 nm.

The specific surface area (SSA) of the composite aerogel was obtained by dynamic N_2 adsorption measurements at −196 °C, using a Nova Quantachrome 4200e instrument analyzer and evaluated by the BET method.

Field emission scanning electron microscopy (FE-SEM) enabled the morphological analysis of the aerogel pellet. A ZEISS MERLIN instrument (Oberkochen, Germany) was used; the samples were deposited on a carbon-coated stub and then coated with a 7 nm Pt layer.

In order to investigate the presence and distribution of FZ powders throughout the aerogel sample, energy-dispersive X-ray spectroscopy (EDS) analyses by using Aztec Software (Oxford Instruments) were performed on the same instrumentation.

Temperature programmed reduction (TPR-H_2) measurements were carried out in AMI-300 (Altamira Instrument). The FZ sample was reduced in 5 % H_2–95 % Ar with a flow rate of 50 N cm^3 min^{-1} and a heating rate of 10 °C min^{-1}. TPR-H_2 profile was recorded using a thermo-conductive detector [69].

2.5. Photocatalytic activity tests

The photocatalytic tests were out carried in presence of UV light using a Pyrex cylindrical reactor (ID = 3.5 cm, h = 28 cm, V = 269 mL). A UV-LEDs strip (nominal power: 10 W, main wavelength emission: 365 nm, provided by LED lighting hut, Shenzhen, China) was used as light source. The UV-LEDs strip was placed around and in contact with the outer surface of the photoreactor. The photocatalytic tests were performed on 100 mL of aqueous solution at a lindane concentration of 100 μg/L and using a photocatalyst dosage equal to 0.09 g/L for FZ, Fe^0 and ZnS in powder form, whereas the used FZsPS dosage was 3 g/L (corresponding to an FZ dosage of 0.09 g/L). Fe^0 degradation efficiency was instead analysed in the absence of light [39].

In the case of the tests with the FZsPS monolithic composite aerogel, a volume (2 mL) of solution was taken at different times to analyze the lindane concentration. In the case of the tests with powder photocatalysts, before the analysis, the taken suspension (2 mL) was filtered through 0.45 μm membrane to separate the photocatalyst from the solution. An Agilent Gas Chromatograph (model 7820 A) equipped with an Electron Capture Detector (ECD) was used to evaluate the lindane concentration. The used analytical method was that one described by the EPA (U.S. Environmental Protection Agency, SW-846 Test Method 8081B, Organochlorine Pesticides by Gas Chromatography). The total organic carbon (TOC) of aqueous solutions was measured with a TOC analyzer (Multi N/C 3100S, Analytik Jena), which used an air flow of 160 Ncm^3/min and drew 500 μL per sample.

2.6. Bioassays and toxicity data analysis

The bioassays carried out with *Artemia franciscana* and data analysis were in accordance with [70,71]. Ten nauplii, metanauplii, and juvenile, and five adults were exposed to increasing percentage concentrations of three experimental conditions ((i) negative control – synthetic seawater (SSW, prepared in according to ISO 10253/16) plus amendments (distilled water + FZ or distilled water + FZsPS); (ii) positive control – seawater spiked with lindane (100 μg/L) (distilled water + lindane) to check the toxic impact of lindane; (iii) seawater spiked with treatments effluents (distilled water + lindane + Fe^0 or distilled water + lindane + FZ or distilled water + lindane + FZsPS or distilled water + lindane + Fe^0sPS or distilled water + lindane + ZsPS).

About RNA extraction and cDNA synthesis, two hundred nauplii and metanauplii, one hundred juvenile and ten adults of *Artemia franciscana* were exposed to 100 % non-diluted aqueous solutions of distilled water + FZsPS, distilled water + lindane and distilled water + lindane + FZsPS. All details about the experimental plan and materials are provided in Supplementary Materials.

3. Results and discussion

3.1. Characterization results

The WAXD results of the FZsPS aerogel (before and after use) and the FZ photocatalyst in powder form are shown in Figure S2 of Supplementary Material. The WAXD spectrum of bare sPS has been included for comparison.

The diffraction patterns of the FZsPS composite aerogel show both the diffraction peaks of the δ crystalline form of sPS (2θ = 10—23.6°) [62] and of the crystalline phase of ZnS (2θ = 28.6, 47.7, 56.6°) [39]. Moreover, the characteristic peak of Fe^0 (2θ = 45°) [39] is also detectable for both FZ and FZsPS composite aerogel, confirming the presence of FZ photocatalyst within the sPS matrix and evidencing that the inclusion of FZ particles within the polymer framework did not alter the δ crystalline form of sPS.

FZsPS specific surface area (SSA), evaluated by BET method, was 309 m^2/g, while for FZ photocatalyst in powder form and bare sPS, the SSA was 44 and 340 m^2/g, respectively. The observed slight reduction of the FZsPS composite SSA compared to that of bare sPS aerogel, as a result of the photocatalyst particle embedding within the sPS framework, is in agreement with SSA values commonly observed in sPS aerogel-based composite materials [39].

Morphological evaluation performed on the FZsPS aerogel by means of Field Emission Scanning Electron Microscopy (FESEM) confirmed the presence of FZ photocatalyst throughout the sample. FESEM images, shown in Fig. 1, highlight the distribution and morphology of FZ powders in FZsPS aerogel.

At lower magnification (Fig. 1A) the sample overview shows that FZ particles are well dispersed and incorporated into the polymer matrix, although particle agglomerates are also present in some areas. At higher magnification (Fig. 1B) the morphology of FZ particles and porosity of the polymeric phase, having a fibrillar structure [66] are better highlighted. The FZ particle morphology observed in the composite, is different from that of the unsupported FZ powders (Figure S3 of Supplementary Material), characterized by sphere-like aggregates composed of flakes. This difference may be ascribed to the processing conditions involved during aerogel formation [72].

EDS analysis on the FZsPS composite aerogel sample was exploited to confirm the chemical composition of the material where the mapping of the different elements composing the catalyst powders enabled to explore their distribution onto the aerogel surface.

As shown in Fig. 2, elements such as Zn, S, Fe and O were found in the FZ particle agglomerates, while C was localized in surrounding area corresponding to the sPS polymeric matrix. The mapping of Fe, Zn and S has highlighted both a homogeneous distribution of these elements and an interpenetration of them, although areas with higher Fe concentrations are also present. The homogeneous interpenetration of Fe and ZnS is in agreement with the distribution of elements observed in unsupported FZ powders (Figure S4 of Supplementary Material), where the EDS elemental analysis highlights the tendency of iron to organize itself in chain structures surrounding the ZnS, phase. Finally, the EDS mapping also evidenced greater concentrations of O in areas characterized by higher Fe concentrations, suggesting the possible presence of iron in its oxidized form.

In order to ascertain the presence of oxidised iron, the FZ sample was studied by means of the TPR technique. The TPR profile of FZ presents reduction peaks located at high temperature, 690 and 740 °C (Fig. 3). These peaks can be attributed exclusively to iron phases, in agreement with the results of Dutková et al [73]. Before 650 °C no reduction peaks are detected, indicating that α-hematite like phase (Fe_2O_3) is not present. Considering the adopted heating ramp (10 °C min^{-1}), the sharp peaks around 700 °C are mainly attributed to the step reduction of the magnetite-like phase (Fe_3O_4) to metallic iron [74]. Correlating this result with the absence of peaks related to iron oxides from the WAXD analysis reported by Sacco et al. [39], we can speculate the presence of

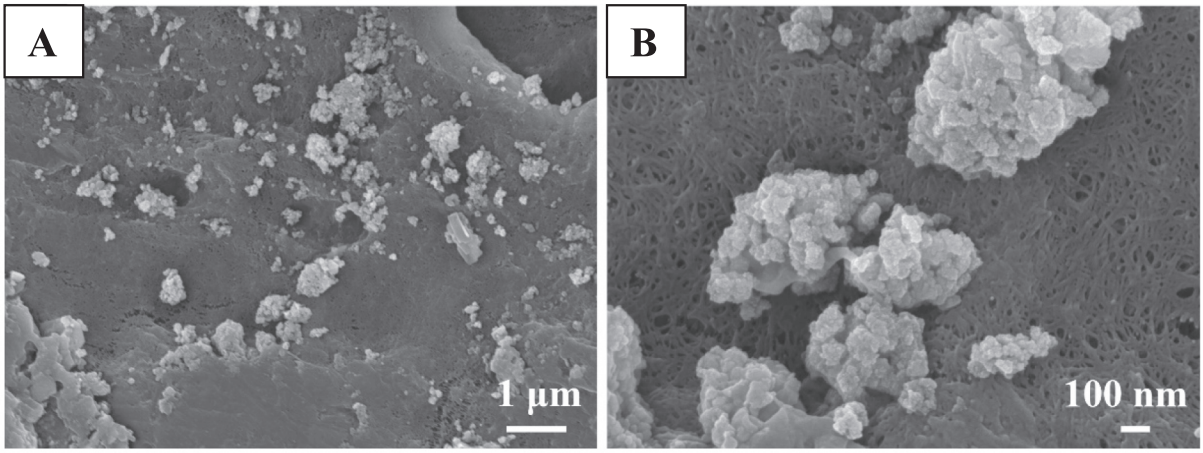

Fig. 1. FESEM images of the FZsPS monolithic composite aerogel at two different magnifications.

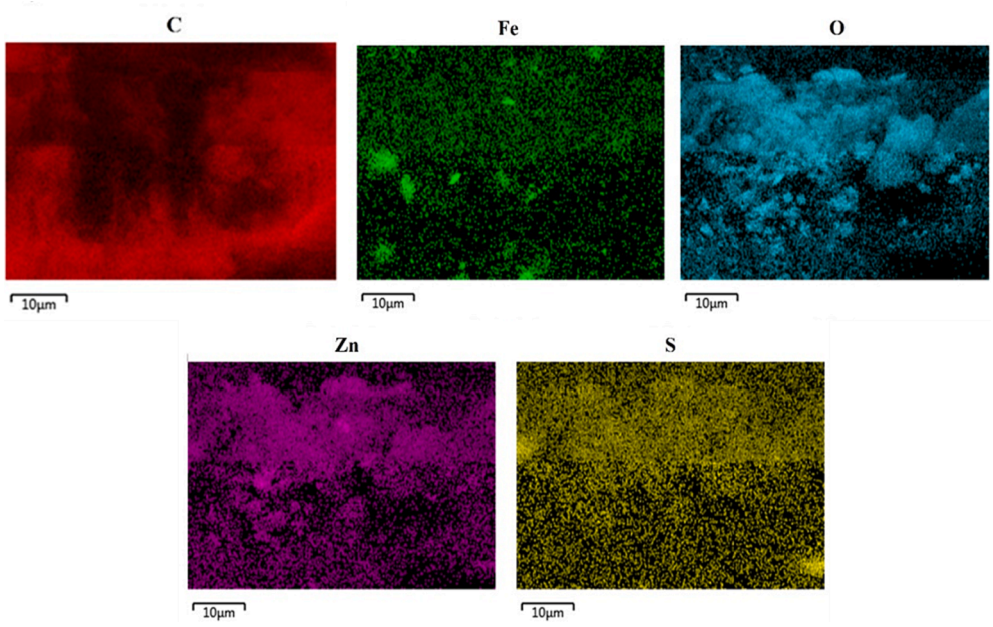

Fig. 2. EDS analysis performed on the composite aerogel FZsPS. Mapping of Fe, O, C, Zn and S elements.

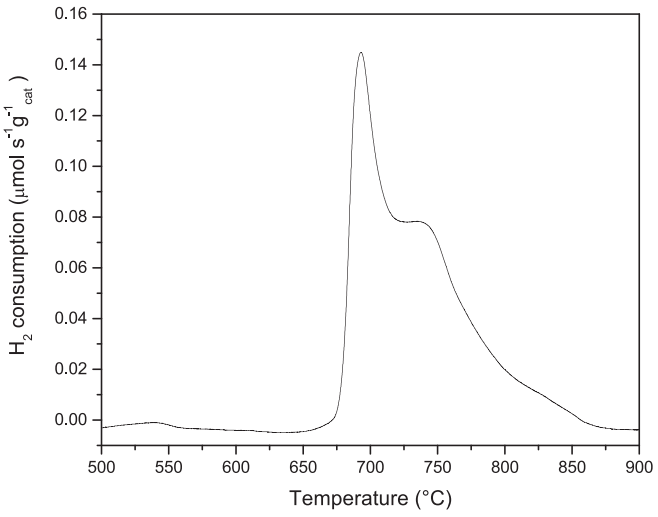

Fig. 3. Temperature programmed reduction (TPR) profile of FZ photocatalyst.

nonstoichiometric amorphous phases. The results obtained from TPR profile agree with the presence of iron oxides detected in the Raman spectrum of FZ reported in ref [39].

Photoluminescence (PL) spectral analysis was conducted to verify the impact of iron on the optical properties of the prepared photocatalyst.

Fig. 4 shows the room temperature PL spectra, under 285 nm excitation, for pure ZnS and FZ powder prepared as reported by Sacco et al. [39]. The PL spectrum of ZnS shows a multipeak emission typical of this semiconductor [75]. The blue emission band is attributed to defect states due to sulfur and zinc vacancies (about 425 and 480 nm, respectively). The broad emission band of peaks located between 360 nm and 405 nm is generally attributed to interstitial defects (S interstitial at low wavelength and Zn interstitial at higher wavelength) [76]. When the iron is introduced into the system, the PL peaks slightly shift to shorter wavelengths [77] but the main effect is the reduction of their intensity. The doping with iron allows to capture the photoactivated electrons and thus slows down the recombination between the valence and conduction bands, resulting in the decrease of PL intensity [78].

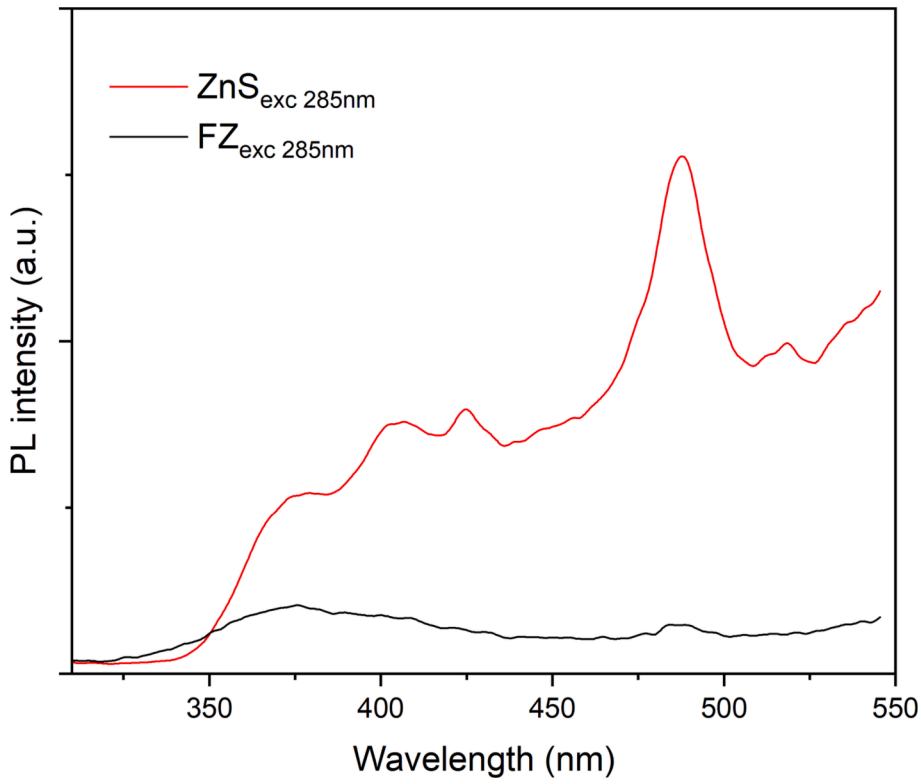

Fig. 4. Photoluminescence spectra of modified and unmodified system: FZ and ZnS.

3.2. Photocatalytic activity results

The photocatalytic activity of commercial ZnS and FZ in powder form was evaluated in the degradation of lindane under UV light irradiation and compared with the degradation efficiency of Fe^0 in the absence of light (Fig. 5). A sample-free control test, performed to verify the contribution of photolysis, showed no influence during the overall irradiation time, while a decrease in lindane relative concentration was found in the presence of ZnS, Fe^0 and FZ. In detail, with ZnS, the lindane concentration slowly decreased as a function of irradiation time, achieving a degradation efficiency of only about 35 % after 180 min. The low photocatalytic activity of ZnS could be explained considering that the C-Cl bonds of lindane structure are difficult to break by hydroxyl radicals generated when ZnS is excited by UV light [39,79,80], as also reported in some literature papers [33,81,82] in which it is shown that the photodegradation efficiency decreases by increasing the number of C-Cl bonds of the pollutants structure. Noticeably, in the absence of UV light, the lindane degradation efficiency by Fe^0 particles was higher than that of ZnS under irradiation, because of the high ability of Fe^0 to break the C-Cl bond of chlorinated organic pollutants [39,83], leading to the complete lindane degradation in 180 min. It is worth to pointing out that, under UV light, the lindane degradation by FZ photocatalyst was enhanced, showing faster degradation kinetics as compared with Fe^0 alone. Indeed, in the presence of FZ photocatalyst and UV light, the lindane relative concentration was always lower than that achieved with the non-irradiated Fe^0 particles. It is argued that the higher lindane degradation efficiency of FZ photocatalyst under UV light is due to the continuous reduction of Fe^{2+} (continuously generated from the reductive cleavage of C-Cl bonds by Fe^0) to Fe^0 by the electrons promoted in the conduction band of photoexcited ZnS, similarly to what reported for the photocatalytic degradation of chlorobenzene in presence of Fe^0/ZnS [39]. This assumption is consistent with the outcomes of photoluminescence analyses, which show a decrease in the electron-hole recombination rate for sample FZ.

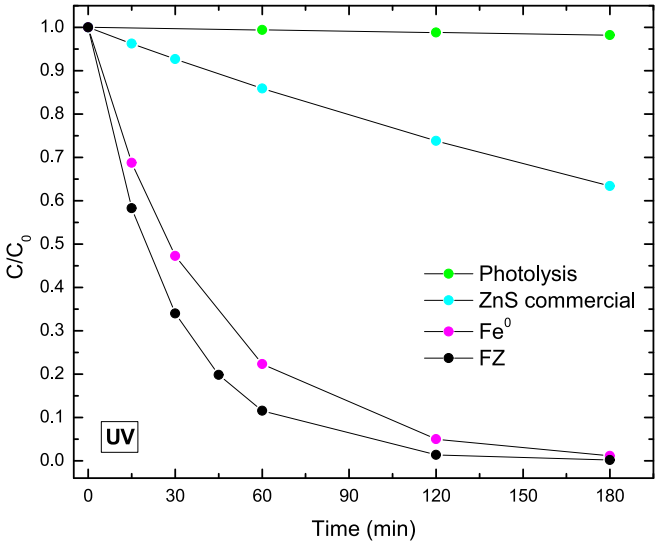

Fig. 5. Photocatalytic degradation of lindane by ZnS and FZ under UV light irradiation and in the presence of Fe^0 in the absence of light.

Fig. 6 reports the comparison of the lindane photocatalytic degradation obtained in the presence of FZ photocatalyst in powder form and FZsPS monolithic composite aerogel.

Despite both FZ powder and FZsPS composite completely degraded lindane after 180 min of UV irradiation, the decreasing rate of lindane relative concentration as a function of irradiation time clearly evidenced a photodegradation activity of FZsPS significantly higher than that observed in the presence of FZ photocatalyst. Indeed, using the FZsPS aerogel, the lindane degradation was about 95 % after only 30 min of irradiation time whereas the FZ photocatalyst exhibited a lindane degradation of about 65 % after the same irradiation time. These data underline that the photodegradation activity is strongly promoted when the FZ photocatalyst in powder form is dispersed in the polymer matrix.

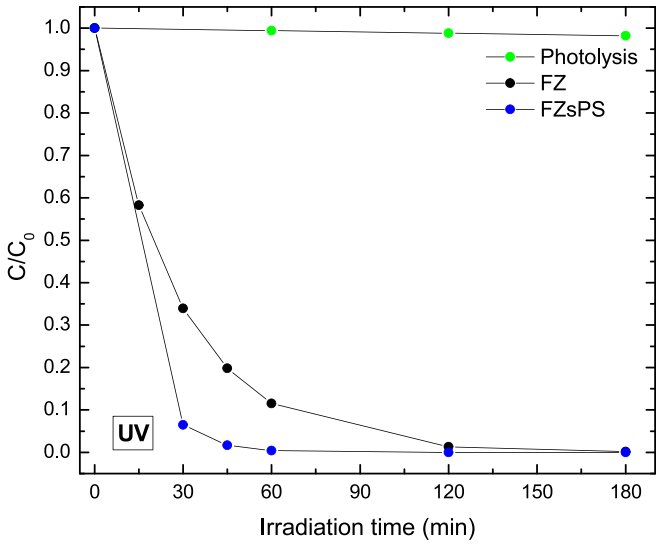

Fig. 6. Photocatalytic degradation of lindane by FZ and FZsPS under UV light irradiation.

The enhanced photocatalytic activity observed in the presence of FZsPS could be due to the higher SSA of FZsPS (309 m^2/g) with respect to FZ (44 m^2/g) but also to the affinity of lindane with the non-polar polymer matrix, which results in a concentration of lindane in the matrix itself. To confirm such hypothesis, an additional experiment was carried out to measure the amount of lindane absorbed by bare sPS monolithic aerogel in dark conditions performed with the same experimental conditions used for the photodegradation tests (solution volume: 100 mL; initial lindane concentration: 100 μg/L; sPS dosage: 3 g/L). (Figure S5 of Supplementary Materials). sPS aerogel showed an uptake of 30 % after 180 min. This result confirms the good affinity of the polymer matrix towards non-polar organic compounds (such as lindane), in agreement with the available literature [61,65,84,85]. Therefore, it is possible to argue that the higher photodegradation efficiency of FZsPS aerogel is mainly due to the lindane absorption ability of the polymer matrix since the number of lindane molecules in contact with FZ particles embedded into sPS aerogel is increased. Thus, the photocatalytic degradation rate is enhanced.

The aqueous solution recovered after the photocatalytic treatment with the FZsPS aerogel was analysed by inductively coupled plasma optical emission spectrometry (ICP-OES Optima 7000DV, PerkinElmer). This analysis revealed the almost total absence of Fe (<0.01 mg/l) and a slight presence of Zn (3 mg/L), probably due to the partial leaching of the FZ particles immobilized on the external surface of sPS and not of those dispersed within the polymer framework.

To test whether such leaching phenomenon could negatively affect the stability of the FZsPS aerogel, photocatalytic experiments were repeated six times (Fig. 7) using the same FZsPS monolithic composite aerogel and without any regeneration step of the photocatalyst.

The obtained results did not evidence any significant decrease in the lindane photocatalytic degradation performance, demonstrating the stability and the possibility of reusing the FZsPS aerogel. Furthermore, WAXD analysis was performed on the FZsPS composite aerogel recovered from the photoreactor after the sixth reuse cycle. The obtained result is shown in Figure S2 of Supplementary Material. No substantial difference with respect to the WAXD spectrum of FZsPS before its use in the photocatalytic degradation of lindane was observed.

An additional photocatalytic test was carried out with the FZsPS monolithic composite at a higher concentration of the pollutant (10 mg/L). The results were comparable to the test at a concentration of 100 μg/L (Fig. 8).

For both initial lindane concentrations, a TOC removal of about 94 %

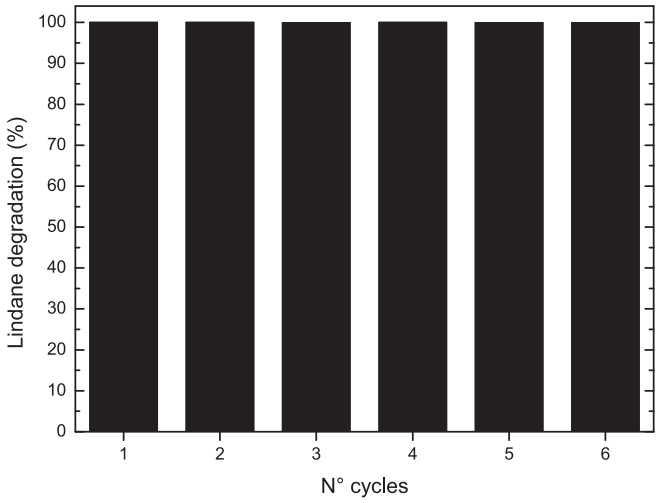

Fig. 7. Lindane degradation after 180 min of UV irradiation using FZsPS aerogel in six reuse cycles.

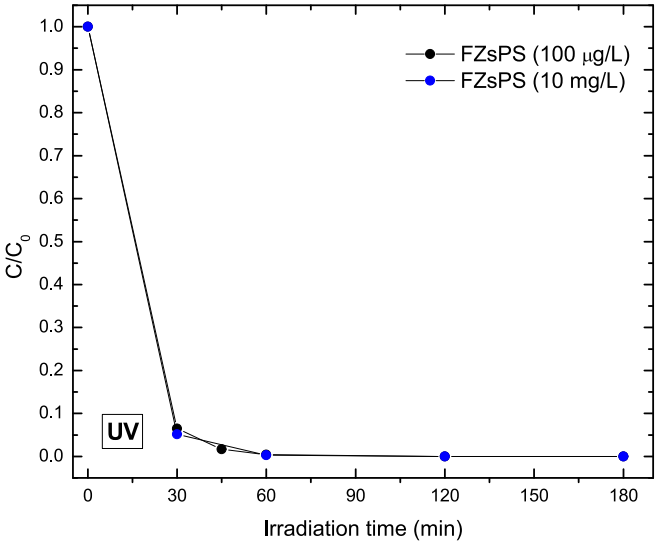

Fig. 8. Photocatalytic degradation at two different lindane initial concentrations (100 μg/L and 10 mg/L) by FZsPS under UV light irradiation.

after 180 min of UV irradiation was achieved, underlining the strong ability of FZsPS in the mineralization of lindane. Considering the literature findings concerning the photoactivity of Fe^0/ZnS in powder form [39], it is possible to argue that the holes generated in the ZnS valence band promote the formation of hydroxyl radicals, which further oxidize the organic intermediates (such as benzene and cyclohexene [86,87]) generated from the cleavage of C-Cl bonds of lindane structure by Fe^0 supported on ZnS surface, leading to the almost complete TOC removal from aqueous solution.

The photocatalytic degradation efficiency of the FZsPS monolithic composite aerogel was compared with the performance of photocatalysts immobilized on different supports and tested in the lindane photodegradation (Table 1).

It is worth noting to underline that the literature about lindane degradation by immobilized photocatalysts is very scarce. However, from the data reported in Table 1, it is possible to observe that the FZsPS monolithic composite aerogel used in our study shows the best performance in lindane degradation since an efficiency of 95 % is reached after only 30 min of irradiation time.

Table 1
Comparison with literature papers dealing with different immobilized photocatalysts for lindane degradation.

Photoactive phase	Support	Light source	Lindane degradation (%)	Treatment time	Ref
TiO_2	Hollow glass microspheres	UV	68	30 min	[27]
N-doped TiO_2	Pyrex glass tube	UVA	~ 20	30 min	[30]
ZnO	Bio-nano hybridsystem (*Candida* VITJzN04).	Sunlight	~ 70	24 h*	[31]
CeO_2–TiO_2	Stainless steel substrates	Simulated solar light	~ 50	2 h*	[88]
Fe^0/ZnS	sPS aerogel	UVA	~ 95	30	This paper

* No data at 30 min is available.

3.3. Toxicity results

As reported in Fig. 9, after 48 h of exposure to different percentages of aqueous solutions of FZsPS, an increase of nauplii, metanauplii, juvenile and adult mortality (about 20 %) was observed only at higher tested percentages, represented by 50 % and 100 %. These data were statistically significant with respect to the control and the others used concentrations ($p < 0.0001$; see Table S1 of Supplementary Material).

Lindane solution (100 μg/L) caused mortality (about 10–20 %) in all life stages already at 6.25 % that was statistically significant with respect to the control and all other concentrations ($p < 0.0001$; Fig. 9; Table S1). Except for adults, the mortality in all life stages at 100 % solution involved all organisms.

Considering nauplii and metanauplii exposure to treated effluent (Lindane + FZsPS) (Fig. 9), a low percentage of about 20 % of dead was observed at 50 %. At 100 %, a significant increase of toxicity (about 30 %) compared to lower (0 %, 6.25 %, 12.5 %, and 25 %; $p < 0.0001$) and higher concentrations (50 %; $p < 0.01$) was detected. Considering juvenile and adult exposure to the same condition, a low percentage of about 20 % of death was observed only at 100 %. These data were statistically significant compared to the control and all other concentrations ($p < 0.0001$; see also Table S1).

Only the 50 % and 100 % of FZ and treated effluent by FZ (Lindane + FZ) (Supplementary Figure S6), caused a significant increase of toxicity in four different life stage (about 20 % and 30 %, respectively) with respect all tested concentrations ($p < 0.0001$).

Taking into the consideration nauplii and metanauplii exposure to treated effluent by Fe^0 (Lindane + Fe^0) at 25 % (Figure S6), a significant percentage of mortality (about 20 % and 35 %, respectively) was observed respecting lower (0 %, 6.25 %, 12.5 %; $p < 0.0001$). At 50 % and 100 %, a significant increase in toxicity (about 40–50 %) was shown respecting all tested concentrations ($p < 0.0001$). Considering juvenile and adult exposure, only at 100 %, Lindane + Fe^0 solution caused a significant increase in mortality (about 40 %) with respect to all tested concentrations ($p < 0.0001$).

Finally, Lindane + Fe^0sPS and Lindane + ZsPS treated effluents (Figure S6) were able to significantly impact the survival of *Artemia* only at 100 % with respect to all tested concentrations ($p < 0.0001$; see also Table S1).

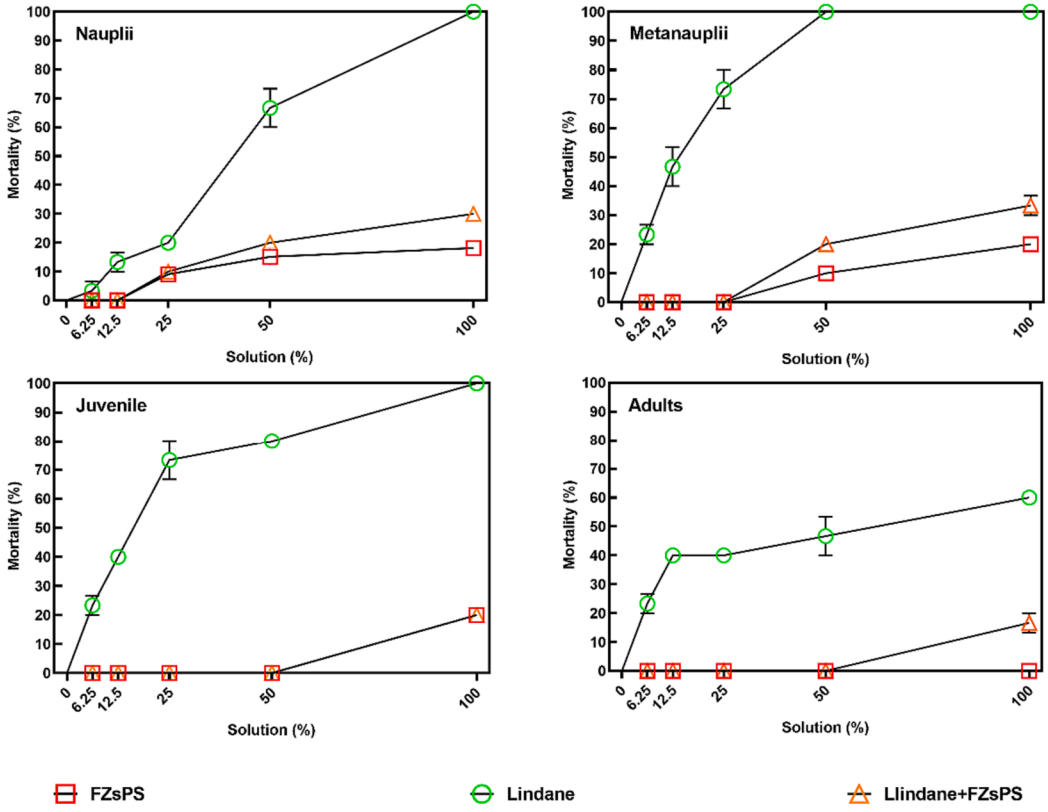

Fig. 9. After 48 h, the percentage of dead nauplii, metanauplii, juvenile and adults detected both in control (0 %) and treated samples with 6.25 %, 12.5 %, 25 %, 50 %, and 100 % of FZsPS solution (distilled water + FZsPS), Lindane solution (100 μg/L), Lindane + FZsPS (Treated effluents after 180 min of UV irradiation). Data are reported as a mean ± standard deviation.

3.4. Effects of FZsPS on gene expression by real-time qPCR

The expression levels of five genes (Albarano et al., 2022a), involved in stress response, were followed by real-time qPCR after FZsPS treatment experiment (Fig. 10; see also Table S2 for the values).

All analyzed genes were targeted in all life stages after lindane exposure with the exception of *hsp60*. Specifically, *hsp26* was down-regulated in nauplii, metanauplii and adult (6.40-fold 2.78-fold and 3.20-fold, respectively) and up-regulated in juvenile (2.46-fold; see Table S2); *hsp70* was down-regulated in nauplii and adult (2.19-fold and 2.87-fold, respectively) and up-regulated in metanauplii and juvenile (2.28-fold and 6.32-fold, respectively); *COXI* and *COXIII* were down-regulated in nauplii (2.77-fold and 7.28-fold, respectively) and metanauplii (2.73-fold and 3.50-fold, respectively) and up-regulated in juvenile (6.91-fold and 2.30-fold, respectively) and adult (9.96-fold and 11.54-fold, respectively; Table S2); *hsp60* was up-regulated in metanauplii, juvenile and adult (2.50-fold, 8.30-fold and 2.90-fold, respectively; see Table S2).

Considering other treatments (Fig. 10), *hsp60* was down-regulated (2.55-fold) only in nauplii after the exposure to the treated effluent (lindane + FZsPS), and *hsp26* was down-regulated (3.01-fold) only in metanauplii after the exposure to FZsPS solution (distilled water + FZsPS) (Table S2).

4. Conclusions

In this work, a monolithic composite aerogel based on sPS and Fe^0/ZnS (FZsPS) was tested, for the first time, as a photocatalyst to achieve the complete lindane degradation under UV light. Fe/ZnS powder is well dispersed throughout the polymer matrix even if agglomerates are present and emerge from the surface, as evident from FESEM images and EDS analysis. The mapping of the different elements (Fe, Zn, S, O, C) showed diffuse Fe chain structures interpenetrated with ZnS particles, although iron oxides, in accordance with TPR analyses, were also detected.

The photodegradation performance of FZsPS was significantly higher than that observed in the presence of Fe^0/ZnS photocatalyst in powder form (FZ). In detail, using the FZsPS monolithic composite aerogel, the almost complete lindane degradation was achieved after only 30 min of irradiation time whereas the FZ photocatalyst exhibited a lindane degradation of about 65 % after the same irradiation time. Moreover, a TOC removal of about 94 % after 180 min of UV irradiation was achieved, underlining the ability of FZsPS also in the lindane mineralization. The enhanced photocatalytic activity observed in the presence of FZsPS aerogel is due to the higher SSA of FZsPS (309 m^2/g) with respect to FZ (44 m^2/g) but also to the concentration of lindane in the sPS matrix. Reusability studies performed on FZsPS showed no significant decrease in the photocatalytic activity, demonstrating the stability of the formulated monolithic composite aerogel. Moreover, the effluent from the photocatalytic treatment based on FZsPs composite aerogel can be considered at low risk of environmental impact since no significant toxic effects on *Artemia franciscana* were evidenced. Therefore, based on the ecotoxicity results, the strategy of dispersing the ZVI/ZnS catalyst in a highly porous polymeric matrix, such as sPS aerogel, can be considered as a model for using otherwise harmful catalysts in water remediation.

CRediT authorship contribution statement

Raffaella Rescigno: Investigation, Methodology, Formal analysis, Writing – original draft. **Olga Sacco:** Conceptualization, Methodology, Supervision, Validation, Writing – review & editing. **Stefania Pragliola:** Writing – review & editing. **Luisa Albarano:** Investigation, Methodology, Formal analysis, Writing – original draft. **Giovanni Libralato:** Conceptualization, Writing – review & editing. **Giusy Lofrano:** Conceptualization, Methodology, Supervision, Validation, Writing – review & editing. **Vincenzo Romano Spica:** Investigation, Methodology, Formal analysis, Writing – original draft. **Olimpia Tammaro:** Investigation, Methodology, Formal analysis, Writing – original draft. **Giorgia Montalbano:** Investigation, Methodology, Formal analysis, Writing – original draft. **Serena Esposito:** Conceptualization, Methodology, Supervision, Validation, Writing – review & editing. **Vincenzo Vaiano:** Conceptualization, Methodology, Supervision, Validation,

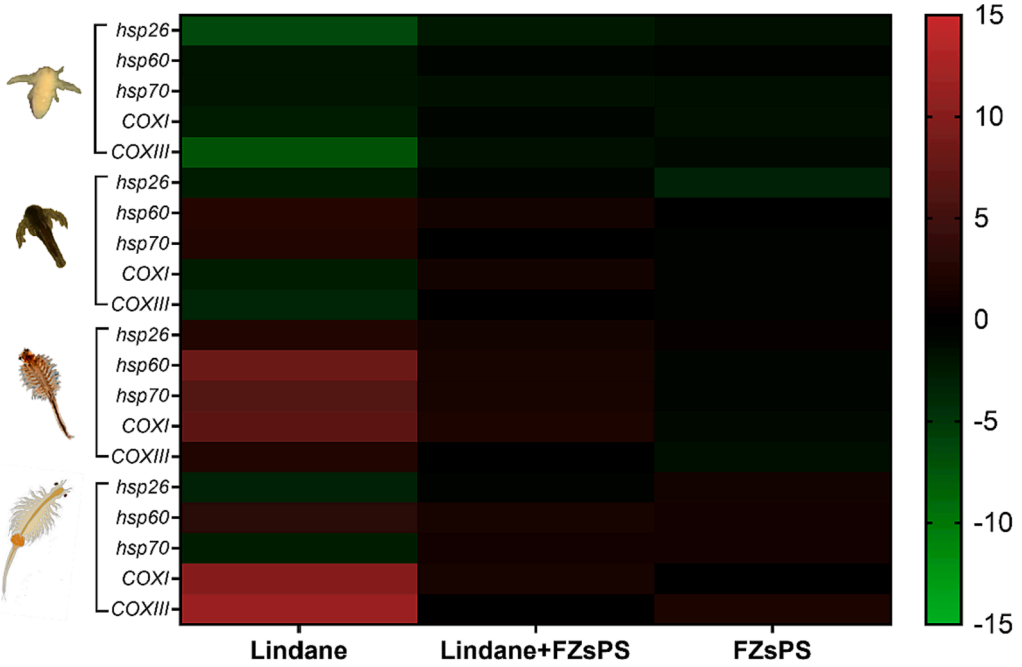

Fig. 10. Heatmap showing the expression profiles and hierarchical clustering of five genes analyzed through real-time qPCR in nauplii, metanauplii, juvenile and adult treated with FZsPS solution (distilled water + FZsPS), Lindane (100 μg/L), Lindane + FZsPS (Treated effluents after 180 min of UV irradiation). Color code: red, up-regulated genes with respect to the control; green, down-regulated genes with respect to the control; black, genes for which there was no variation in expression with respect to the control. (For interpretation of the references to color in this figure legend, the reader is referred to the web version of this article.)

Writing – review & editing. **Vincenzo Venditto:** Conceptualization, Writing – review & editing.

Declaration of Competing Interest

The authors declare that they have no known competing financial interests or personal relationships that could have appeared to influence the work reported in this paper.

Data availability

No data was used for the research described in the article.

Acknowledgements

Authors thank Dr Marco Allione (Politecnico di Torino, Italy) for FESEM measurements on Fe^0/ZnS photocatalyst, Dr. Mariagrazia Napoli and Dr. Ivano Immediata (University of Salerno, Italy) for the technical assistance in gas chromatographic analysis. Authors also thank Dr. Patrizia Iannece (University of Salerno, Italy) for the ICP-OES analysis of water recovered after the photocatalytic treatment.

Appendix A. Supplementary material

Supplementary data to this article can be found online at https://doi.org/10.1016/j.seppur.2023.125246.

References

[1] L.R.E.D. RED, Docket Control Number OPP-2002-0202 Lindane Reregistration Eligibility Decision (RED) Comments Submitted on Behalf of the Natural Resources Defense Council By Gina M. Solomon, MD, MPH Senior Scientist, NRDC, (2002).
[2] H. Fu, X. Quan, Z. Liu, S. Chen, Photoinduced transformation of γ-HCH in the presence of dissolved organic matter and enhanced photoreactive activity of humate-coated α-Fe2O3, Langmuir 20 (2004) 4867–4873.
[3] G. Marko, M. Snezana, B. Jelena, K. Marijana, R. Srdjan, T. Aleksandra, A. Jasmina, Lindane and hexachlorobenzene sequestration and detoxification in contaminated sediment amended with carbon-rich sorbents, Chemosphere (2019).
[4] W.H. Organization, Lindane (gamma-HCH: health and safety guide, (1991).
[5] J. Vijgen, The Legacy of Lindane HCH Isomer Production: A Global Overview of Residue Management, Formulation and Disposal: Main Report, International HCH & Pesticides Association, Annexes, 2006.
[6] M. Vega, D. Romano, E. Uotila, Lindane, Persistant Organic Pollutant) in the EU, Best Practices of De-Contamination Exchanged, 2016.
[7] W.H. Organization, Pesticide Residues in Food-2003: Evaluations, Food & Agriculture Org, 2004.
[8] J.C. Hansen, L.-O. Reiersen, S. Wilson, Arctic Monitoring and Assessment Programme (AMAP); strategy and results with focus on the human health assessment under the second phase of AMAP, 1998–2003, in, Taylor & Francis, 2002.
[9] M. Gmurek, M. Olak-Kucharczyk, S. Ledakowicz, Photochemical decomposition of endocrine disrupting compounds–A review, Chem. Eng. J. 310 (2017) 437–456.
[10] J.O. Babayemi, Overview of levels of organochlorine pesticides in surface water and food items in Nigeria, J. Environ. Earth Sci. 6 (2016) 77–86.
[11] V. Nagpal, A.D. Bokare, R.C. Chikate, C.V. Rode, K.M. Paknikar, Reductive dechlorination of γ-hexachlorocyclohexane using Fe–Pd bimetallic nanoparticles, J. Hazard. Mater. 175 (2010) 680–687.
[12] J. Vijgen, P. Abhilash, Y.F. Li, R. Lal, M. Forter, J. Torres, N. Singh, M. Yunus, C. Tian, A. Schäffer, Hexachlorocyclohexane (HCH) as new Stockholm Convention POPs—a global perspective on the management of Lindane and its waste isomers, Environ. Sci. Pollut. Res. 18 (2011) 152–162.
[13] B.R. Shah, U.D. Patel, Mechanistic aspects of photocatalytic degradation of Lindane by TiO2 in the presence of Oxalic acid and EDTA as hole-scavengers, J. Environ. Chem. Eng. 9 (2021), 105458.
[14] S. Wacławek, D. Silvestri, P. Hrabák, V.V. Padil, R. Torres-Mendieta, M. Wacławek, M. Černík, D.D. Dionysiou, Chemical oxidation and reduction of hexachlorocyclohexanes: A review, Water Res. 162 (2019) 302–319.
[15] S. Deng, N. Feng, S. Kang, J. Zhu, B. Yu, J. Chen, X. Xie, Mechanochemical formation of chlorinated phenoxy radicals and their roles in the remediation of hexachlorobenzene contaminated soil, J. Hazard. Mater. 352 (2018) 172–181.
[16] I. San Román, A. Galdames, M. Alonso, L. Bartolomé, J. Vilas, R. Alonso, Effect of coating on the environmental applications of zero valent iron nanoparticles: the lindane case, Sci. Total Environ. 565 (2016) 795–803.
[17] X. Zhu, Y. Li, B. Han, Q. Feng, L. Zhou, Degradation Characteristics of Carbon Tetrachloride by Granular Sponge Zero Valent Iron, Int. J. Environ. Res. Public Health 18 (2021) 12578.
[18] S. Bajaj, S. Sagar, S. Khare, D.K. Singh, Biodegradation of γ-hexachlorocyclohexane (lindane) by halophilic bacterium Chromohalobacter sp. LD2 isolated from HCH dumpsite, Int. Biodeter. Biodegr. 122 (2017) 23–28.
[19] F.O. Kengara, U. Doerfler, G. Welzl, B. Ruth, J.C. Munch, R. Schroll, Enhanced degradation of 14C-HCB in two tropical clay soils using multiple anaerobic–aerobic cycles, Environ. Pollut. 173 (2013) 168–175.
[20] J.F. Devlin, J. Klausen, R.P. Schwarzenbach, Kinetics of nitroaromatic reduction on granular iron in recirculating batch experiments, Environ. Sci. Tech. 32 (1998) 1941–1947.
[21] H.-J. Lu, J.-K. Wang, S. Ferguson, T. Wang, Y. Bao, H.-X. Hao, Mechanism, synthesis and modification of nano zerovalent iron in water treatment, Nanoscale 8 (2016) 9962–9975.
[22] T. Pasinszki, M. Krebsz, Synthesis and application of zero-valent iron nanoparticles in water treatment, environmental remediation, catalysis, and their biological effects, Nanomaterials 10 (2020) 917.
[23] W. Shen, X. Wang, F. Jia, Z. Tong, H. Sun, X. Wang, F. Song, Z. Ai, L. Zhang, B. Chai, Amorphization enables highly efficient anaerobic thiamphenicol reduction by zero-valent iron, Appl Catal B 264 (2020), 118550.
[24] W. Xu, Z. Li, S. Shi, J. Qi, S. Cai, Y. Yu, D.M. O'Carroll, F. He, Carboxymethyl cellulose stabilized and sulfidated nanoscale zero-valent iron: Characterization and trichloroethene dechlorination, Appl. Catal. B 262 (2020), 118303.
[25] V. Vaiano, O. Sacco, M. Matarangolo, Photocatalytic degradation of paracetamol under UV irradiation using TiO2-graphite composites, Catal. Today 315 (2018) 230–236.
[26] S. Khan, C. Han, M. Sayed, M. Sohail, S. Jan, S. Sultana, H.M. Khan, D. D. Dionysiou, Exhaustive photocatalytic lindane degradation by combined simulated solar light-activated nanocrystalline TiO2 and inorganic oxidants, Catalysts 9 (2019) 425.
[27] A. Zaleska, J. Hupka, M. Wiergowski, M. Biziuk, Photocatalytic degradation of lindane, p, p′-DDT and methoxychlor in an aqueous environment, J. Photochem. Photobiol. A Chem. 135 (2000) 213–220.
[28] H.J. Jung, R. Koutavarapu, S. Lee, J.H. Kim, H.C. Choi, M.Y. Choi, Enhanced photocatalytic degradation of lindane using metal–semiconductor Zn@ ZnO and ZnO/Ag nanostructures, J. Environ. Sci. 74 (2018) 107–115.
[29] D.-K. Lee, I.-C. Cho, Characterization of TiO2 thin film immobilized on glass tube and its application to PCE photocatalytic destruction, Microchem. J. 68 (2001) 215–223.
[30] J. Senthilnathan, L. Philip, Photocatalytic degradation of lindane under UV and visible light using N-doped TiO2, Chem. Eng. J. 161 (2010) 83–92.
[31] J.A. Salam, N. Das, Degradation of lindane by a novel embedded bio-nano hybrid system in aqueous environment, Appl. Microbiol. Biotechnol. 99 (2015) 2351–2360.
[32] T.S. Jamil, E.S. Mansor, R.A. Nasr, Degradation of Lindane using two nanosized BiOXs and their heterojunction under visible light, Desalin. Water Treat. 57 (2016) 14750–14761.
[33] S. Khan, C. Han, H.M. Khan, D.L. Boccelli, M.N. Nadagouda, D.D. Dionysiou, Efficient degradation of lindane by visible and simulated solar light-assisted S-TiO2/peroxymonosulfate process: kinetics and mechanistic investigations, Mol. Catal. 428 (2017) 9–16.
[34] X. Wang, M. Hong, F. Zhang, Z. Zhuang, Y. Yu, Recyclable nanoscale zero valent iron doped g-C3N4/MoS2 for efficient photocatalysis of RhB and Cr (VI) driven by visible light, ACS Sustain. Chem. Eng. 4 (2016) 4055–4063.
[35] X. Wang, D. Lizong, Well-dispersed zero-valent iron supported on Fe_3O_4/gC_3N_4 composites via a facile approach with versatile photoredox catalysis, J. Nanopart. Res. 20 (2018) 1–15.
[36] C. Huang, W.-P. Hsieh, J.R. Pan, S.-M. Chang, Characteristic of an innovative TiO_2/Fe0 composite for treatment of azo dye, Sep. Purif. Technol. 58 (2007) 152–158.
[37] K. Kobwittaya, S. Sirivithayapakorn, Photocatalytic reduction of nitrate over Fe-modified TiO_2, APCBEE Proc. 10 (2014) 321–325.
[38] Y. Liu, J. Wang, Reduction of nitrate by zero valent iron (ZVI)-based materials: A review, Sci. Total Environ. 671 (2019) 388–403.
[39] O. Sacco, V. Vaiano, W. Navarra, C. Daniel, S. Pragliola, V. Venditto, Catalytic system based on recyclable Fe0 and ZnS semiconductor for UV-promoted degradation of chlorinated organic compounds, Sep. Purif. Technol. 270 (2021), 118830.
[40] D. Friedmann, A General Overview of Heterogeneous Photocatalysis as a Remediation Technology for Wastewaters Containing Pharmaceutical Compounds, Water 14 (2022) 3588.
[41] S.K. Loeb, P.J. Alvarez, J.A. Brame, E.L. Cates, W. Choi, J. Crittenden, D. D. Dionysiou, Q. Li, G. Li-Puma, X. Quan, The technology horizon for photocatalytic water treatment: sunrise or sunset? ACS Publ. (2018).
[42] R. Ata, O. Sacco, V. Vaiano, L. Rizzo, G.Y. Tore, D. Sannino, Visible light active N-doped TiO2 immobilized on polystyrene as efficient system for wastewater treatment, J. Photochem. Photobiol. A Chem. 348 (2017) 255–262.
[43] V. Vaiano, G. Sarno, O. Sacco, D. Sannino, Degradation of terephthalic acid in a photocatalytic system able to work also at high pressure, Chem. Eng. J. 312 (2017) 10–19.
[44] I. Zammit, R.B. Marano, V. Vaiano, E. Cytryn, L. Rizzo, Changes in antibiotic resistance gene levels in soil after irrigation with treated wastewater: a comparison between heterogeneous photocatalysis and chlorination, Environ. Sci. Tech. 54 (2020) 7677–7686.
[45] O. Sacco, M. Matarangolo, V. Vaiano, G. Libralato, M. Guida, G. Lofrano, M. Carotenuto, Crystal violet and toxicity removal by adsorption and simultaneous photocatalysis in a continuous flow micro-reactor, Sci. Total Environ. 644 (2018) 430–438.

[46] D. Minetto, G. Libralato, A.V. Ghirardini, Ecotoxicity of engineered TiO2 nanoparticles to saltwater organisms: an overview, Environ. Int. 66 (2014) 18–27.
[47] B.M. Rotoli, P. Guidi, B. Bonelli, M. Bernardeschi, M.G. Bianchi, S. Esposito, G. Frenzilli, P. Lucchesi, M. Nigro, V. Scarcelli, Imogolite: an aluminosilicate nanotube endowed with low cytotoxicity and genotoxicity, Chem. Res. Toxicol. 27 (2014) 1142–1154.
[48] V. Addorisio, D. Pirozzi, S. Esposito, F. Sannino, Decontamination of waters polluted with simazine by sorption on mesoporous metal oxides, J. Hazard. Mater. 196 (2011) 242–247.
[49] F. Tescione, O. Tammaro, A. Bifulco, G. Del Monaco, S. Esposito, M. Pansini, B. Silvestri, A. Costantini, Silica meets tannic acid: Designing green nanoplatforms for environment preservation, Molecules 27 (2022) 1944.
[50] T. McMurray, P. Dunlop, J. Byrne, The photocatalytic degradation of atrazine on nanoparticulate TiO_2 films, J. Photochem. Photobiol. A Chem. 182 (2006) 43–51.
[51] M. Karavasilis, M. Theodoropoulou, C. Tsakiroglou, Degradation of the Persistent Organic Pollutant-Lindane in Fixed-Bed Photoreactor Packed with Immobilized Zinc Oxide and Iron Oxide-Doped Zinc Oxide Photocatalysts, in: IOP Conference Series: Earth and Environmental Science, IOP Publishing, 2022, p. 012082.
[52] V. Venditto, M. Pellegrino, R. Califano, G. Guerra, C. Daniel, L. Ambrosio, A. Borriello, Monolithic polymeric aerogels with VOCs sorbent nanoporous crystalline and water sorbent amorphous phases, ACS Appl. Mater. Interfaces 7 (2015) 1318–1326.
[53] C. Daniel, M. Pellegrino, V. Venditto, S. Aurucci, G. Guerra, Nanoporous-crystalline poly (2, 6-dimethyl-1, 4-phenylene) oxide (PPO) aerogels, Polymer 105 (2016) 96–103.
[54] G. Balasubramanian, D.D. Dionysiou, M.T. Suidan, I. Baudin, J.-M. Laıné, Evaluating the activities of immobilized TiO2 powder films for the photocatalytic degradation of organic contaminants in water, Appl Catal B 47 (2004) 73–84.
[55] S. Suárez, J.M. Coronado, R. Portela, J.C. Martín, M. Yates, P. Avila, B. Sánchez, On the preparation of TiO2– sepiolite hybrid materials for the photocatalytic degradation of TCE: influence of TiO2 distribution in the mineralization, Environ. Sci. Tech. 42 (2008) 5892–5896.
[56] O. Sacco, V. Vaiano, M. Matarangolo, ZnO supported on zeolite pellets as efficient catalytic system for the removal of caffeine by adsorption and photocatalysis, Sep. Purif. Technol. 193 (2018) 303–310.
[57] S. Singh, H. Mahalingam, P.K. Singh, Polymer-supported titanium dioxide photocatalysts for environmental remediation: A review, Appl. Catal. A 462 (2013) 178–195.
[58] M.J. Silva, J. Gomes, P. Ferreira, R.C. Martins, An overview of polymer-supported catalysts for wastewater treatment through light-driven processes, Water 14 (2022) 825.
[59] W. Navarra, O. Sacco, C. Daniel, V. Venditto, V. Vaiano, D.A.L. Vignati, C. Bojic, G. Libralato, G. Lofrano, M. Carotenuto, Photocatalytic degradation of atrazine by an N-doped TiO2/polymer composite: catalytic efficiency and toxicity evaluation, J. Environ. Chem. Eng. 10 (2022), 108167.
[60] S. Pragliola, R. De Vita, P. Longo, Aqueous emulsion polymerization of styrene and substituted styrenes using titanocene compounds, Polymer 54 (2013) 1583–1587.
[61] C. Daniel, S. Longo, R. Ricciardi, E. Reverchon, G. Guerra, Monolithic nanoporous crystalline aerogels, Macromol. Rapid Commun. 34 (2013) 1194–1207.
[62] V. Vaiano, O. Sacco, D. Sannino, P. Ciambelli, S. Longo, V. Venditto, G. Guerra, N-doped TiO2/s-PS aerogels for photocatalytic degradation of organic dyes in wastewater under visible light irradiation, J. Chem. Technol. Biotechnol. 89 (2014) 1175–1181.
[63] A. Mancuso, V. Vaiano, P. Antico, O. Sacco, V. Venditto, Photoreactive polymer composite for selective oxidation of benzene to phenol, Catal. Today 413 (2023), 113914.
[64] W. Navarra, O. Sacco, V. Venditto, V. Vaiano, Selective Photocatalytic Reduction of Nitrobenzene to Aniline Using TiO2 Embedded in sPS Aerogel, Polymers 15 (2023) 359.
[65] O. Sacco, V. Vaiano, C. Daniel, W. Navarra, V. Venditto, Highly robust and selective system for water pollutants removal: How to transform a traditional photocatalyst into a highly robust and selective system for water pollutants removal, Nanomaterials 9 (2019) 1509.
[66] O. Sacco, V. Vaiano, C. Daniel, W. Navarra, V. Venditto, Removal of phenol in aqueous media by N-doped TiO2 based photocatalytic aerogels, Mater. Sci. Semicond. Process. 80 (2018) 104–110.
[67] V. Vaiano, O. Sacco, D. Sannino, Enhanced photocatalytic degradation of organic pollutants in wastewater using photocatalysts coupled with luminescent materials, Chem. Eng. Trans. 60 (2017) 211–216.
[68] O. Sacco, V. Vaiano, D. Sannino, R. Picca, N. Cioffi, Ag modified ZnS for photocatalytic water pollutants degradation: Influence of metal loading and preparation method, J. Colloid Interface Sci. 537 (2019) 671–681.
[69] G. Bagnasco, C. Cammarano, M. Turco, S. Esposito, A. Aronne, P. Pernice, TPR/TPO characterization of cobalt–silicon mixed oxide nanocomposites prepared by sol–gel, Thermochim Acta 471 (2008) 51–54.
[70] L. Albarano, S. Serafini, M. Toscanesi, M. Trifuoggi, V. Zupo, M. Costantini, D. A. Vignati, M. Guida, G. Libralato, Genotoxicity Set Up in Artemia franciscana Nauplii and Adults Exposed to Phenanthrene, Naphthalene, Fluoranthene, and Benzo (k) fluoranthene, Water 14 (2022) 1594.
[71] L. Albarano, M. Toscanesi, M. Trifuoggi, M. Guida, G. Lofrano, G. Libralato, In situ microcosm remediation of polyaromatic hydrocarbons: influence and effectiveness of Nano-Zero Valent Iron and activated carbon, Environ. Sci. Pollut. Res. 30 (2023) 3235–3251.
[72] M. Pansini, G. Dell'Agli, A. Marocco, P.A. Netti, E. Battista, V. Lettera, P. Vergara, P. Allia, B. Bonelli, P. Tiberto, Preparation and characterization of magnetic and porous metal-ceramic nanocomposites from a zeolite precursor and their application for DNA separation, J. Biomed. Nanotechnol. 13 (2017) 337–348.
[73] E. Dutková, P. Baláž, P. Pourghahramani, S. Velumani, J. Ascencio, N. Kostova, Properties of mechanochemically synthesized ZnS nanoparticles, J. Nanosci. Nanotechnol. 9 (2009) 6600–6605.
[74] W. Jozwiak, E. Kaczmarek, T. Maniecki, W. Ignaczak, W. Maniukiewicz, Reduction behavior of iron oxides in hydrogen and carbon monoxide atmospheres, Appl. Catal. A 326 (2007) 17–27.
[75] D. Denzler, M. Olschewski, K. Sattler, Luminescence studies of localized gap states in colloidal ZnS nanocrystals, J. Appl. Phys. 84 (1998) 2841–2845.
[76] K.N. Devi, T.S. Chanu, L.A. Chanu, W.J. Singh, K.J. Singh, Operational parameters and major active species responsible for the photodegradation of malachite green dye by ZnO/ZnS core–shell nanocomposite photocatalyst, J. Mater. Res. 38 (2023) 473–483.
[77] S. Horoz, O. Sahin, Investigations of structural, optical, and photovoltaic properties of Fe-alloyed ZnS quantum dots, J. Mater. Sci. Mater. Electron. 28 (2017) 9559–9565.
[78] S. Kumar, N. Verma, Structural, optical and magnetic investigations on Fe-doped ZnS nanoparticles, J. Mater. Sci. Mater. Electron. 26 (2015) 2754–2759.
[79] W. He, H. Jia, J. Cai, X. Han, Z. Zheng, W.G. Wamer, J.-J. Yin, Production of reactive oxygen species and electrons from photoexcited ZnO and ZnS nanoparticles: a comparative study for unraveling their distinct photocatalytic activities, J. Phys. Chem. C 120 (2016) 3187–3195.
[80] L. Isac, A. Enesca, Recent Developments in ZnS-Based Nanostructures Photocatalysts for Wastewater Treatment, Int. J. Mol. Sci. 23 (2022) 15668.
[81] L.O. Conte, S. Cotillas, A. Sánchez-Yepes, D. Lorenzo, A. Santos, LED visible light assisted photochemical oxidation of HCHs in aqueous phases polluted with DNAPL, Process Saf. Environ. Prot. 168 (2022) 434–442.
[82] S. Khan, X. He, J.A. Khan, H.M. Khan, D.L. Boccelli, D.D. Dionysiou, Kinetics and mechanism of sulfate radical-and hydroxyl radical-induced degradation of highly chlorinated pesticide lindane in UV/peroxymonosulfate system, Chem. Eng. J. 318 (2017) 135–142.
[83] B. Gunawardana, N. Singhal, P. Swedlund, Degradation of chlorinated phenols by zero valent iron and bimetals of iron: a review, Environ. Eng. Res. 16 (2011) 187–203.
[84] C. Daniel, D. Sannino, G. Guerra, Syndiotactic polystyrene aerogels: adsorption in amorphous pores and absorption in crystalline nanocavities, Chem. Mater. 20 (2008) 577–582.
[85] A. Mancuso, O. Sacco, V. Venditto, W. Navarra, P. Antico, C. Daniel, V. Vaiano, Selective Absorption of Aromatic Compounds by Syndiotactic Polystyrene Aerogels, in: Macromolecular Symposia, Wiley Online Library, 2023, p. 2200062.
[86] C. Chang, F. Lian, L. Zhu, Simultaneous adsorption and degradation of γ-HCH by nZVI/Cu bimetallic nanoparticles with activated carbon support, Environ. Pollut. 159 (2011) 2507–2514.
[87] Z. Wang, W. Huang, Dechlorination of γ-hexachlorocyclohexane by zero-valent metallic iron, J. Hazard. Mater. 166 (2009) 992–997.
[88] N. Radić, B. Grbić, S. Stojadinović, M. Ilić, O. Došen, P. Stefanov, TiO2–CeO2 composite coatings for photocatalytic degradation of chloropesticide and organic dye, J. Mater. Sci. Mater. Electron. 33 (2022) 5073–5086.